Editors' Suggestion

Vacancy-Induced Tunable Kondo Effect in Twisted Bilayer Graphene

Yueqing Chang,[1,2,*] Jinjing Yi,[1,2] Ang-Kun Wu,[1,2] Fabian B. Kugler,[3,1,2] Eva Y. Andrei,[1] David Vanderbilt,[1,2] Gabriel Kotliar,[1,2,4] and J. H. Pixley[1,2,3,†]

[1]*Department of Physics and Astronomy, Rutgers University, Piscataway, New Jersey 08854, USA*
[2]*Center for Materials Theory, Rutgers University, Piscataway, New Jersey 08854, USA*
[3]*Center for Computational Quantum Physics, Flatiron Institute, 162 5th Avenue, New York, New York 10010, USA*
[4]*Condensed Matter Physics and Materials Science Department, Brookhaven National Laboratory, Upton, New York 11973, USA*

(Received 7 January 2024; revised 3 July 2024; accepted 18 August 2024; published 19 September 2024)

In single sheets of graphene, vacancy-induced states have been shown to host an effective spin-1/2 hole that can be Kondo screened at low temperatures. Here, we show how these vacancy-induced impurity states survive in twisted bilayer graphene (TBG), which thus provides a tunable system to probe the critical destruction of the Kondo effect in pseudogap hosts. *Ab initio* calculations and atomic-scale modeling are used to determine the nature of the vacancy states in the vicinity of the magic angle in TBG, demonstrating that the vacancy can be treated as a quantum impurity. Utilizing this insight, we construct an Anderson impurity model with a TBG host that we solve using the numerical renormalization group combined with the kernel polynomial method. We determine the phase diagram of the model and show how there is a strict dichotomy between vacancies in the AA/BB versus AB/BA tunneling regions. In AB/BA vacancies, the Kondo temperature at the magic angle develops a broad distribution with a tail to vanishing temperatures due to multifractal wave functions at the magic angle. We argue that scanning tunneling microscopy in the vicinity of the vacancy can act as a probe of both the critical single-particle states and the underlying many-body ground state in magic-angle TBG.

DOI: 10.1103/PhysRevLett.133.126503

Twisted van der Waals heterostructures have taken the condensed matter community by storm [1–4]. Since the first experimental evidence of the band reconstruction and emergence of a flat band in twisted bilayer graphene (TBG) at twist angle $\sim 1°$ [5], a wide range of experimental and technical breakthroughs [6–9] have paved the way for the discovery and reproducible observations of correlated insulating states [10] and superconductivity [11] in magic-angle TBG, highlighting the vast potential and intriguing properties of these moiré materials [12–37]. These ideas have now been extended to twisted bilayer transition metal dichalcogenides (TMD) [38–42], quantum magnets [43,44], high-temperature superconductors [45–49], and bosonic superfluids in optical lattices [50–53]. To unravel the nature of the underlying many-body states in moiré materials, it is essential to explore new ways to extract electron correlations while using current experimental capabilities.

One potentially fruitful direction is to probe the nature of impurity states, accurately measurable with scanning tunneling microscopy (STM), to gain insights into the many-body ground state that the impurity states are coupled to. For instance, tunneling spectra of impurity-induced resonances in superconductors reveal signatures of the pairing symmetry [54]. For single sheets of graphene, creating impurity states strongly coupled to the itinerant electrons was a challenge until it was realized that vacancy-induced bound states act like a spin-1/2 hole, originating from the vacancy's nearest-neighbor σ states which couple to the π band due to the local curvature near the vacancy site [55–60]. This represents a clear-cut realization of the pseudogap Anderson impurity model (AIM), which features a quantum critical point at nonzero Kondo coupling [61–73]. Yet, experimentally observing this quantum critical point has remained out of reach due to the lack of tunability of vacancy states, despite the observation of Kondo screening in graphene hosts [59,74].

In this work, we study vacancy-induced impurity states in TBG away from and at the magic angle with atomic-scale and effective lattice models. Using *ab initio* calculations, we show that a vacancy [75] induces an effective spin-1/2 hole on the atomic scale and compute the hybridization between the vacancy and the twisted pair of π bands, showing a clear dichotomy between AA/BB and AB/BA regions. This is in stark contrast to the recent description of TBG as a topological Kondo lattice problem with suitably defined "impurity" limits (i.e., realizing local moments on the moiré scale) [30–37,76]. Here, we focus on atomic-scale vacancies that arise in realistic experimental settings across a wide array of moiré materials

*Contact author: yueqing.chang@rutgers.edu
†Contact author: jed.pixley@physics.rutgers.edu

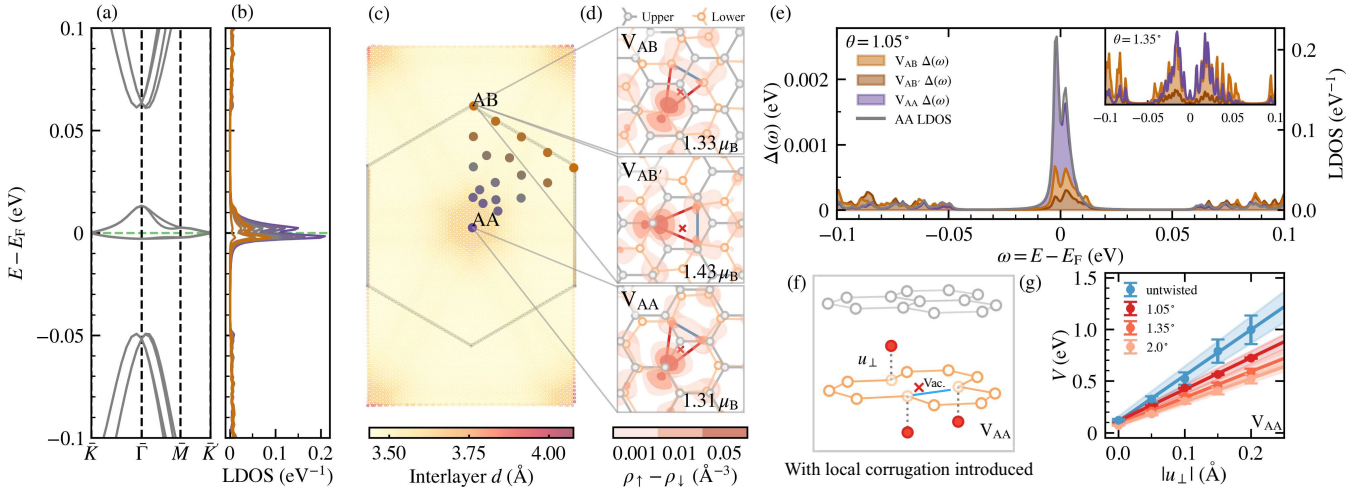

FIG. 1. Atomic-scale modeling of TBG with a vacancy. (a) Band structure of pristine TBG at θ_M without vacancy. $\bar{K}$ and $\bar{K}'$ indicate the two valleys of the moiré Brillouin zone. (b) Projected local density of states (LDOS) at the potential vacancy sites denoted in (c), color coded. (c) The C atoms in the relaxed pristine TBG at θ_M, with the center of AA and AB regions annotated. The atoms are colored coded according to the local interlayer spacing. The hexagon represents the moiré unit cell. The 19 potential vacancy sites chosen for computing the LDOS in (b) are indicated by thicker dots. (d) $\rho_\uparrow - \rho_\downarrow$ for three typical vacancy configurations, computed in untwisted bilayer graphene using DFT. V_{AB} and $V_{AB'}$ vacancies could be present in TBG AB regions, while V_{AA} vacancies are typical in AA regions. The gray (orange) circles denote the C atoms in the upper (lower) layers, and the red cross denotes the vacancy. The blue (red) lines highlight the shorter (longer) distances between three adjacent sites. The clouds of $\rho_\uparrow - \rho_\downarrow$ are plotted in red, showing that most of the excessive spin is contributed by the σ lobe at the isolated adjacent site. (e) Hybridization function at θ_M between the V_σ state and the TBG bath for the three vacancy configurations. The LDOS for the AA site is also plotted in the gray curve for comparison. The insets show the hybridization at $\theta = 1.35°$, which features a Dirac-cone-like low-energy dispersion with larger flat-band bandwidth compared to 1.05°. (f) Side view of AA-stacked bilayer graphene near the vacancy site, with manual vertical displacements of the three adjacent sites away from equilibrium, denoted by $u_\perp$. The bonded sites (connected by a blue line) are displaced downward by the same $u_\perp$. (g) Hybridization strength V between the V_σ state and the bath versus $u_\perp$ for the untwisted V_{AA} vacancy (blue) and when coupled to the TBG bath (red). Lines are linear fits, showing that V is tunable by $u_\perp$ and θ.

(e.g., graphene [77], TMD [78,79], cuprate superconductors [80,81]). We use *ab initio* derived vacancy states to construct an effective quantum impurity model for a realistic vacancy, which is solved by combining the kernel polynomial method [82] and the numerical renormalization group [83] (KPM + NRG [84]). Away from the magic angle, this realizes a tunable, pseudogap AIM where twisting the bilayers tunes the vacancy through its quantum phase transition. At the magic angle, the impurity is always Kondo screened at low temperatures. We study the distribution of Kondo temperatures T_K across the sample to show how T_K in the AB region is strongly suppressed relative to the AA region.

Microscopic picture—To set the stage, we investigate how the vacancy σ (V_σ) state in TBG at the magic angle ($\theta_M = 1.05°$ [85]) hybridizes with the twisted pair of π bands using an accurate machine-learned tight-binding model [86], combined with embedded V_σ states from density functional theory (DFT) calculations [87]. Figure 1(c) shows the structure of TBG at θ_M obtained by fully relaxing freestanding TBG using the interatomic potential model [110–112] with the method described in Refs. [113,114], using the molecular dynamics (MD) simulation package LAMMPS [115]. The in-plane and out-of-plane atomic relaxations manifest in enlarged AB/BA regions, consistent with previous work [113,114,116–119]. Figure 1(a) shows the band structure of fully relaxed pristine TBG in the atomic-scale tight-binding model, and Fig. 1(b) the local density of states (LDOS) projected onto the potential vacancy sites indicated in panel (c). The flat-band states are mostly localized in the AA regions (except at Γ) and have decreasing projections onto sites further away from the AA center. This indicates that an impurity in the AA (AB) regions hybridizes more (less) with the localized flat-band states.

To understand microscopically how vacancy states hybridize with the π bands in TBG, we first consider a monovacancy in single-layer graphene. Removing one atom leaves dangling vacancy V_π and V_σ orbitals at the three adjacent atoms, which undergo a Jahn–Teller distortion so that one isolated atom moves further away from the vacancy, and the other two atoms move closer to rebond. This leads to one V_σ state localized at the isolated site near the Fermi level and a V_π quasilocalized zero mode [56,57]. In the experimentally relevant regime, the effect of the V_π zero mode can be qualitatively captured by a renormalization of the V_σ Coulomb interaction [59]; we thus focus on the V_σ state in the following.

In single-layer graphene, the coupling between the V_σ state and the π bands requires finite local corrugation that breaks the mirror symmetry [59,60]. This coupling arises naturally if a second, untwisted layer is stacked onto freestanding graphene, which breaks the mirror symmetry near the vacancy site in the lower layer. To capture this, we performed DFT calculations using a 6×6 supercell of freestanding untwisted bilayer graphene with one vacancy in the bottom layer in three typical local environments [87], named after the registry of the two sheets of graphene. Note that, in AB-stacked graphene, there are two types of vacancies, V_{AB} and $V_{AB'}$ [see Fig. 1(d)]. Similar to single-layer graphene, the three adjacent atoms near the vacancy site relax to a final equilibrium configuration with almost no corrugation near the vacancy. Figure 1(d) shows the calculated excessive spin density, $\rho_\uparrow - \rho_\downarrow$ [120], which is centered at the isolated adjacent C atom, contributed mainly by the σ-lobe toward the vacancy. The details of the calculations and the electronic structure of bilayer graphene with a vacancy are summarized in [87].

In the dilute limit, we expect the 6×6 supercell simulation of the V_σ state in untwisted bilayer graphene to mimic the actual vacancy in TBG near θ_M. Using our DFT results in untwisted bilayer graphene, we compute the hybridization function between the dangling V_σ state and the "bath" (TBG *without* the vacancy and its three adjacent sites) from the microscopic model, $\Delta_{\text{micro}}(\omega) = \pi \sum_{n,\mathbf{k}} |V_{n\mathbf{k}}|^2 \delta(\omega - \epsilon_{n\mathbf{k}})$. Here, $V_{n\mathbf{k}} = \langle \phi_{V_\sigma} | H_{V_\sigma\text{-bath}} \mathcal{P}_{\text{bath-TBG}} | \psi_{n\mathbf{k}} \rangle$ represents the tunneling matrix element between the V_σ state $|\phi_{V_\sigma}\rangle$ and the pristine TBG eigenstate $|\psi_{n\mathbf{k}}\rangle$ with eigenvalue $\epsilon_{n\mathbf{k}}$. $H_{V_\sigma\text{-bath}}$ is the hopping between the V_σ state and the C atoms in the bath; $\mathcal{P}_{\text{bath-TBG}}$ projects the TBG eigenstate from the Hilbert space of N-site TBG to that of the $(N-1)$-orbital π bath. Figure 1(e) shows $\Delta_{\text{micro}}(\omega)$ for the three vacancy environments at θ_M and the LDOS at the AA center, with insets showing the result at 1.35°. In comparison, V_{AA} hybridizes much stronger with the bath, especially with the flat-band states.

In experiments, the substrate almost always induces local corrugation in TBG, which is not captured in our MD simulations. Therefore, we manually introduced local corrugation near the vacancy to study how it changes the hybridization. Figure 1(f) shows a schematic side view of how the three vacancy-adjacent atoms are displaced by $u_\perp$ either upward or downward [87] for a V_{AA} vacancy. Figure 1(g) shows that the hybridization strength V increases with $u_\perp$ and decreases with θ. For $u_\perp > 0.2$ Å, a localized V_σ state can no longer be identified. We find that V_{AA} vacancies are more sensitive to twisting [87].

In summary, a vacancy in bilayer graphene induces a localized spin density, which hybridizes with the π bath with a strength tunable via the local environment, atomic corrugation, and the twist angle, suggesting that TBG with a monovacancy realizes a tunable, pseudogap AIM. To make the AIM tractable, we construct an effective model with the impurity parameters derived from the microscopic model and the hybridization function from a simpler TBG bath. The latter has all of the salient features we have just found and allows us to describe the spectral properties of TBG down to sufficiently low energy scales to treat the Kondo effect accurately.

Quantum impurity model—We use the AIM, with the Hamiltonian $H = H_{\text{host}} + H_{\text{hyb}} + H_{\text{imp}}$, to emulate TBG with a vacancy. The host contributions are typically written in the single-particle eigenbasis, where ϵ_k is the eigenenergy of a state created by $c^\dagger_{k\sigma}$ with a wave function $\phi_{k\sigma}(j) = \langle j, \sigma | \epsilon_k \rangle$ at lattice site j [121]. Then,

$$H_{\text{host}} = \sum_{k,\sigma} \epsilon_k c^\dagger_{k\sigma} c_{k\sigma}, \quad H_{\text{hyb}} = V \sum_\sigma \left(d^\dagger_\sigma c_{R\sigma} + \text{H.c.} \right), \quad (1)$$

where R labels the impurity site, $c_{R\sigma} = \sum_k \phi_k(R) c_{k\sigma}$, and $V > 0$ is the hybridization strength. The effect of the host on the impurity is described by the hybridization function

$$\Delta_R(\omega) = \pi V^2 \sum_k |\phi_k(R)|^2 \delta(\omega - \epsilon_k) \equiv \pi V^2 \rho_R(\omega), \quad (2)$$

with ρ_R the host LDOS per spin orientation ($\phi_k \equiv \phi_{k\sigma}$). One approximation we consider to help gain physical insight into the problem ignores the spatial contribution of the wave function to the LDOS, so that the LDOS in the hybridization function is replaced by the global DOS (GDOS, per spin orientation, per lattice site) $\rho(\omega) = N^{-1} \sum_k \delta(\omega - \epsilon_k)$.

To describe the ω dependence of $\Delta_R(\omega)$, we use a microscopic lattice model of TBG [122] derived from the Bistritzer–MacDonald (BM) continuum model [85,87], which can be scaled up in system size, provides higher resolution for the ultralow-energy features in the LDOS and captures the emergent multifractality in TBG's wave functions at θ_M [87]. We can modify $\Delta_R(\omega)$ by varying either the twist angle θ or the interlayer tunneling w, since only their ratio matters at small twist angles in the form $\alpha \equiv w/[2 v_F k_D \sin(\theta/2)]$. Here, the Fermi velocity is $v_F = 3 t a_0/(2\hbar)$ with $t = 2.8$ eV, and the distance from the Γ to the Dirac point is $k_D = 4\pi/(3a_0)$ with $a_0 \approx 2.46$ Å the graphene lattice constant. It is more convenient for us to vary w at fixed $\theta = 1.05°$ as we treat the incommensurate twist via a rational approximation. The magic angle α_M then occurs at $w = 0.11$ eV.

We focus on the charge neutrality point and show the DOS of the TBG lattice model in Fig. 2(a). Relaxation in the lattice model is accounted for by breaking the symmetry in the tunneling between the AA and AB regions, with $w_{AA}/w_{AB} = 0.75$ [123]. In the BM model, the GDOS can have a charge neutrality van Hove singularity at the magic angle, which (ignoring how the impurity is embedded in

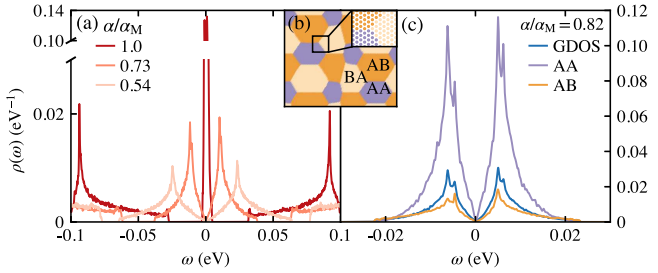

FIG. 2. Hybridization functions for the effective lattice model of TBG in Eq. (1). (a) The model GDOS at different twist parameters, where $\alpha = 0.081$ ($w = 0.11$ eV) corresponds to the magic angle. (b) Tunneling map, where different colors indicate the locally dominating tunneling according to the effective lattice model [87]. The inset shows the microscopic lattice spacing across a patch. (c) Comparison of GDOS and LDOS in the AA and AB regions at $\alpha = 0.067$ ($w = 0.09$ eV). The LDOS is averaged over 200 samples of random twisted boundary conditions; the GDOS is additionally averaged over the origin of rotation in TBG across 400 samples.

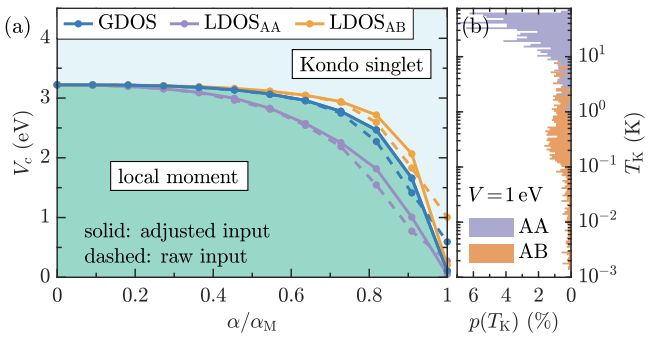

FIG. 3. Solution of the quantum impurity model. (a) Phase diagram at $T = 0$. The critical hybridization strength V_c that separates the local-moment ($\mu_{\text{eff}} = 1/4$) and Kondo-singlet phase ($\mu_{\text{eff}} = 0$) as a function of $\alpha = w/[2v_F k_D \sin(\theta/2)]$ vanishes linearly at the magic angle $\alpha_M \approx 1/\sqrt{3}$ [cf. Eq. (4)]. Dashed lines show results for $\Delta \propto \rho$ with the GDOS ρ or with an LDOS ρ_R (R in the AA or AB region), see Eq. (2). For the solid lines, the input is adjusted to match the analytically known asymptotic low-energy behavior [87]. (b) Distribution of T_K for different impurity locations across magic-angle TBG. We consider $V = 1$ eV and roughly 500 (1500) sites for the AA (AB) region. The AB, compared to the AA distribution, is broader, centered at a smaller value, and has a tail reaching down to very low T_K.

the host) leads to Kondo screening of the impurity [76]. Incorporating the impurity location, the tunneling strengths in the lattice model mark different sublattice tunneling geometries dominated by AA/BB or AB/BA regions [Fig. 2(b)]. The LDOS in each representative region, depicted in Fig. 2(c) away from α_M, reflects how the probability density of wave functions in the miniband are concentrated near the AA sites, consistent with our atomic-scale model results [87] and expectations from previous TBG Wannier-function calculations [14,15,124–126].

Finally, the impurity part in the Hamiltonian reads

$$H_{\text{imp}} = \epsilon_d(\hat{n}_{d\uparrow} + \hat{n}_{d\downarrow}) + U\hat{n}_{d\uparrow}\hat{n}_{d\downarrow}. \tag{3}$$

An impurity state with spin σ and on-site repulsion U, localized at the vacancy site R, is created by $d_\sigma^\dagger$, has a number operator $\hat{n}_{d\sigma} = d_\sigma^\dagger d_\sigma$, and an energy ϵ_d measured from the host Fermi energy $E_F = 0$. We choose $U = 2.2$ eV and $\epsilon_d = -0.5$ eV as motivated by our microscopic analysis [87]. Note that the hybridization functions already break particle-hole symmetry and that the TBG half bandwidth (of the full spectrum, not only the miniband) D depends weakly on α, $D(\alpha) \approx 8$ eV. Below, the hybridization strength is either varied or chosen as $V = 1$ eV to estimate the typical T_K. The effective Kondo coupling is $J \sim V^2/U$.

Many-body solution—We first consider the $T = 0$ phase diagram for a vacancy in TBG with variable hybridization strength V and twist parameter α. A single sheet of graphene realizes a clear-cut pseudogap AIM with a local-moment and Kondo-singlet phase. Away from α_M, the GDOS of TBG still follows the pseudogap behavior: at low energies, $\rho(\omega) \sim |\omega|/v^2$, where $v = v(\alpha)$ is the renormalized Dirac velocity. As $v(\alpha)$ vanishes at α_M ($\alpha_M \approx 1/\sqrt{3}$ for the first magic angle in [85]), we may expand it as $v(\alpha) \sim |\alpha - \alpha_M|$ close to α_M. From previous NRG studies, we know that such a particle-hole asymmetric pseudogap AIM has a critical Kondo coupling J_c with $\rho_0 J_c \sim \mathcal{O}(1)$ [63–65,70,127]. Hence, from $\rho_0 \sim 1/v^2(\alpha)$, we expect

$$J_c \sim |\alpha - \alpha_M|^2 \Leftrightarrow V_c \sim |\alpha - \alpha_M|. \tag{4}$$

At α_M, $\rho(\omega)$ is smooth at low ω with finite $\rho(0)$. Hence, at $T = 0$, a Kondo-singlet phase is found for arbitrarily small V.

We use KPM with a linear lattice size $L = 569a_0$ [122] and an expansion order of $N_C = 2^{18}$ to calculate the Wilson-chain coefficients. Then, from the NRG impurity contribution to the spin susceptibility χ_{imp}, we extract the effective magnetic moment $\mu_{\text{eff}} = \lim_{T\to 0} T\chi_{\text{imp}}(T)$. This yields a phase diagram, Fig. 3(a), where the local-moment and Kondo-singlet phases are characterized by $\mu_{\text{eff}} = 1/4$ and $\mu_{\text{eff}} = 0$, respectively. $V_c(\alpha)$ for hybridization functions proportional to an LDOS (with R in either the AA or AB region) and to the GDOS (equivalent to the R-averaged LDOS) behave qualitatively similarly. As expected, in the AA region, the enhanced LDOS leads to a smaller V_c relative to the AB/BA regions. For the GDOS, we can use the asymptotic low-energy behavior mentioned before ($\rho(\omega)|_{\alpha\neq\alpha_M} \sim |\omega|$, $\rho(\omega)|_{\alpha_M} = \text{const}$) to adjust and extend the Wilson-chain input at energy scales below the KPM resolution [87]. The data with adjusted input nicely reproduces Eq. (4) and confirms our expectations: There is a finite V_c for all $\alpha \neq \alpha_M$, decreasing linearly with α close to α_M. At $\alpha = \alpha_M$, any $V > 0$ leads to Kondo

screening, consistent with a recent study using the GDOS in TBG [76].

Focusing on α_M, where the ground state is always Kondo-screened, we may ask below which T the Kondo-singlet phase occurs across the sample, i.e., how T_K changes with the location of the impurity at fixed V (say, 1 eV). We use $T_K \simeq 1/|4\chi_{loc}|$ [128] as a robust and efficient estimate, where $\chi_{loc} = \partial_h \langle S^z \rangle|_{h=0}$ (with $\langle S^z \rangle$ the local magnetization) is the local susceptibility computed at $T = 0$. In Fig. 3(b), we plot the distribution of Kondo scales found for a large number of different sites. There is a strict dichotomy between vacancies in the AA versus AB regions. The LDOS throughout the AA region is rather similar, leading to a narrow distribution of Kondo scales. By contrast, the LDOS in the AB region varies widely at low energies (as it includes V_{AB} and $V_{AB'}$ contributions) and is generally smaller than in the AA region. This leads to a broad distribution of Kondo scales, centered at a smaller value than in the AA region, and with a tail to vanishing T_K. This tail is a signature of a broad distribution we expect [84,129–131] to result from the multifractal wave functions at the magic angle that arise in several incommensurate models of TBG [51,132] including H_{host} in Eq. (1) (see [87]).

In reality, the TBG bath becomes correlated very close to θ_M, and the noninteracting bath description breaks down. Therefore, at $T = 0$, our results are directly applicable across the majority of the phase diagram in Fig. 3(a), while future work is needed to incorporate the strongly correlated bath that can induce a gap at charge neutrality [133]. At finite temperatures above the correlated gap, our results serve as a description of the normal state of the defect-induced Kondo effect in TBG.

Conclusion—Using *ab initio* calculations, we embedded a vacancy into pristine TBG and demonstrated how it hybridizes with the low-energy miniband in the vicinity of the magic angle. From this insight, we built an effective AIM that we solved with KPM + NRG [84]. We found a variety of many-body ground states and a pseudogap quantum critical point tunable by the twist angle. At the magic angle, the vacancy is always Kondo screened, leading to a distribution of Kondo temperatures that is broad in the AB region due to the underlying multifractal single-particle eigenstates [51,132]. We propose the STM response of such Kondo-induced vacancy states as a probe of the underlying many-body ground states in TBG and moiré materials more broadly.

Acknowledgments—We thank Kevin Ingersent and Justin Wilson for insightful discussions and collaborations on related work. Y. C. thanks Tawfiqur Rakib for help in setting up MD simulations for TBG, and Shang Ren and Michele Pizzochero for valuable discussions. This work has been supported in part by the NSF CAREER Grant No. DMR 1941569 (A. K. W., J. H. P.), the BSF Grant No. 2020264 (J. Y., J. H. P.), the Alfred P. Sloan Foundation through a Sloan Research Fellowship (J. H. P.), Department of Energy DOE-FG02-99ER45742 (E. Y. A.), the Gordon and Betty Moore Foundation EPiQS initiative GBMF9453 (E. Y. A.), the NSF Grant No. DMR 1954856 (D. V.), and the U.S. Department of Energy, Office of Science, Office of Advanced Scientific Computing Research, and Office of Basic Energy Sciences, Scientific Discovery through Advanced Computing (SciDAC) program (G. K.). F. B. K. acknowledges support by the Alexander von Humboldt Foundation through the Feodor Lynen Fellowship. Y. C. acknowledges support from the Abrahams Postdoctoral Fellowship of the Center for Materials Theory at Rutgers University. The Flatiron Institute is a division of the Simons Foundation.

Data availability—The KPM computations were performed using the Beowulf cluster at the Department of Physics and Astronomy of Rutgers University and the Amarel cluster provided by the Office of Advanced Research Computing (OARC) [134] at Rutgers, The State University of New Jersey. The NRG results were obtained using the QSpace tensor library developed by A. Weichselbaum [135] and the NRG toolbox by Seung-Sup B. Lee [136–138].

[1] E. Y. Andrei and A. H. MacDonald, Graphene bilayers with a twist, Nat. Mater. **19**, 1265 (2020).
[2] L. Balents, C. R. Dean, D. K. Efetov, and A. F. Young, Superconductivity and strong correlations in moiré flat bands, Nat. Phys. **16**, 725 (2020).
[3] E. Y. Andrei, D. K. Efetov, P. Jarillo-Herrero, A. H. MacDonald, K. F. Mak, T. Senthil, E. Tutuc, A. Yazdani, and A. F. Young, The marvels of moiré materials, Nat. Rev. Mater. **6**, 201 (2021).
[4] K. P. Nuckolls and A. Yazdani, A microscopic perspective on moiré materials, Nat. Rev. Mater. **9**, 460 (2024).
[5] G. Li, A. Luican, J. M. B. Lopes Dos Santos, A. H. Castro Neto, A. Reina, J. Kong, and E. Y. Andrei, Observation of van Hove singularities in twisted graphene layers, Nat. Phys. **6**, 109 (2010).
[6] A. Luican, G. Li, A. Reina, J. Kong, R. R. Nair, K. S. Novoselov, A. K. Geim, and E. Y. Andrei, Single-layer behavior and its breakdown in twisted graphene layers, Phys. Rev. Lett. **106**, 126802 (2011).
[7] W. Yan, M. Liu, R.-F. Dou, L. Meng, L. Feng, Z.-D. Chu, Y. Zhang, Z. Liu, J.-C. Nie, and L. He, Angle-dependent van Hove singularities in a slightly twisted graphene bilayer, Phys. Rev. Lett. **109**, 126801 (2012).
[8] K. Kim, M. Yankowitz, B. Fallahazad, S. Kang, H. C. P. Movva, S. Huang, S. Larentis, C. M. Corbet, T. Taniguchi, K. Watanabe, S. K. Banerjee, B. J. LeRoy, and E. Tutuc, van der Waals heterostructures with high accuracy rotational alignment, Nano Lett. **16**, 1989 (2016).
[9] Y. Cao, J. Y. Luo, V. Fatemi, S. Fang, J. D. Sanchez-Yamagishi, K. Watanabe, T. Taniguchi, E. Kaxiras, and P. Jarillo-Herrero, Superlattice-induced insulating states and

valley-protected orbits in twisted bilayer graphene, Phys. Rev. Lett. **117**, 116804 (2016).
[10] Y. Cao, V. Fatemi, A. Demir, S. Fang, S. L. Tomarken, J. Y. Luo, J. D. Sanchez-Yamagishi, K. Watanabe, T. Taniguchi, E. Kaxiras, R. C. Ashoori, and P. Jarillo-Herrero, Correlated insulator behaviour at half-filling in magic-angle graphene superlattices, Nature (London) **556**, 80 (2018).
[11] Y. Cao, V. Fatemi, S. Fang, K. Watanabe, T. Taniguchi, E. Kaxiras, and P. Jarillo-Herrero, Unconventional superconductivity in magic-angle graphene superlattices, Nature (London) **556**, 43 (2018).
[12] D. K. Efimkin and A. H. MacDonald, Helical network model for twisted bilayer graphene, Phys. Rev. B **98**, 035404 (2018).
[13] C. Xu and L. Balents, Topological superconductivity in twisted multilayer graphene, Phys. Rev. Lett. **121**, 087001 (2018).
[14] J. Kang and O. Vafek, Symmetry, maximally localized wannier states, and a low-energy model for twisted bilayer graphene narrow bands, Phys. Rev. X **8**, 031088 (2018).
[15] M. Koshino, N. F. Q. Yuan, T. Koretsune, M. Ochi, K. Kuroki, and L. Fu, Maximally localized Wannier orbitals and the extended Hubbard model for twisted bilayer graphene, Phys. Rev. X **8**, 031087 (2018).
[16] B. Padhi, C. Setty, and P. W. Phillips, Doped twisted bilayer graphene near magic angles: Proximity to Wigner crystallization, not Mott insulation, Nano Lett. **18**, 6175 (2018).
[17] F. Guinea and N. R. Walet, Electrostatic effects, band distortions, and superconductivity in twisted graphene bilayers, Proc. Natl. Acad. Sci. U.S.A. **115**, 13174 (2018).
[18] G. Tarnopolsky, A. J. Kruchkov, and A. Vishwanath, Origin of magic angles in twisted bilayer graphene, Phys. Rev. Lett. **122**, 106405 (2019).
[19] J. Liu, J. Liu, and X. Dai, Pseudo Landau level representation of twisted bilayer graphene: Band topology and implications on the correlated insulating phase, Phys. Rev. B **99**, 155415 (2019).
[20] J. Kang and O. Vafek, Strong coupling phases of partially filled twisted bilayer graphene narrow bands, Phys. Rev. Lett. **122**, 246401 (2019).
[21] M. Xie and A. H. MacDonald, Nature of the correlated insulator states in twisted bilayer graphene, Phys. Rev. Lett. **124**, 097601 (2020).
[22] N. Bultinck, E. Khalaf, S. Liu, S. Chatterjee, A. Vishwanath, and M. P. Zaletel, Ground state and hidden symmetry of magic-angle graphene at even integer filling, Phys. Rev. X **10**, 031034 (2020).
[23] O. Vafek and J. Kang, Renormalization group study of hidden symmetry in twisted bilayer graphene with Coulomb interactions, Phys. Rev. Lett. **125**, 257602 (2020).
[24] B. A. Bernevig, Z.-D. Song, N. Regnault, and B. Lian, Twisted bilayer graphene. I. Matrix elements, approximations, perturbation theory, and a $k \cdot p$ two-band model, Phys. Rev. B **103**, 205411 (2021).
[25] Z.-D. Song, B. Lian, N. Regnault, and B. A. Bernevig, Twisted bilayer graphene. II. Stable symmetry anomaly, Phys. Rev. B **103**, 205412 (2021).
[26] B. A. Bernevig, Z.-D. Song, N. Regnault, and B. Lian, Twisted bilayer graphene. III. Interacting Hamiltonian and exact symmetries, Phys. Rev. B **103**, 205413 (2021).
[27] B. Lian, Z.-D. Song, N. Regnault, D. K. Efetov, A. Yazdani, and B. A. Bernevig, Twisted bilayer graphene. IV. Exact insulator ground states and phase diagram, Phys. Rev. B **103**, 205414 (2021).
[28] B. A. Bernevig, B. Lian, A. Cowsik, F. Xie, N. Regnault, and Z.-D. Song, Twisted bilayer graphene. V. Exact analytic many-body excitations in Coulomb Hamiltonians: Charge gap, Goldstone modes, and absence of Cooper pairing, Phys. Rev. B **103**, 205415 (2021).
[29] O. Vafek and J. Kang, Lattice model for the Coulomb interacting chiral limit of magic-angle twisted bilayer graphene: Symmetries, obstructions, and excitations, Phys. Rev. B **104**, 075143 (2021).
[30] Z.-D. Song and B. A. Bernevig, Magic-angle twisted bilayer graphene as a topological heavy fermion problem, Phys. Rev. Lett. **129**, 047601 (2022).
[31] H. Hu, B. A. Bernevig, and A. M. Tsvelik, Kondo lattice model of magic-angle twisted-bilayer graphene: Hund's rule, local-moment fluctuations, and low-energy effective theory, Phys. Rev. Lett. **131**, 026502 (2023).
[32] Y.-Z. Chou and S. Das Sarma, Kondo lattice model in magic-angle twisted bilayer graphene, Phys. Rev. Lett. **131**, 026501 (2023).
[33] D. Călugăru, M. Borovkov, L. L. H. Lau, P. Coleman, Z.-D. Song, and B. A. Bernevig, Twisted bilayer graphene as topological heavy fermion: II. Analytical approximations of the model parameters, Low Temp. Phys. **49**, 640 (2023).
[34] L. L. H. Lau and P. Coleman, Topological mixed valence model for twisted bilayer graphene, arXiv:2303.02670.
[35] G.-D. Zhou, Y.-J. Wang, N. Tong, and Z.-D. Song, Kondo phase in twisted bilayer graphene, Phys. Rev. B **109**, 045419 (2024).
[36] Y.-Z. Chou and S. Das Sarma, Scaling theory of intrinsic Kondo and Hund's rule interactions in magic-angle twisted bilayer graphene, Phys. Rev. B **108**, 125106 (2023).
[37] H. Hu, G. Rai, L. Crippa, J. Herzog-Arbeitman, D. Călugăru, T. Wehling, G. Sangiovanni, R. Valentí, A. M. Tsvelik, and B. A. Bernevig, Symmetric Kondo lattice states in doped strained twisted bilayer graphene, Phys. Rev. Lett. **131**, 166501 (2023).
[38] F. Wu, T. Lovorn, E. Tutuc, and A. H. MacDonald, Hubbard model physics in transition metal dichalcogenide moiré bands, Phys. Rev. Lett. **121**, 026402 (2018).
[39] E. C. Regan, D. Wang, C. Jin, M. I. Bakti Utama, B. Gao, X. Wei, S. Zhao, W. Zhao, Z. Zhang, K. Yumigeta, M. Blei, J. D. Carlström, K. Watanabe, T. Taniguchi, S. Tongay, M. Crommie, A. Zettl, and F. Wang, Mott and generalized Wigner crystal states in WSe_2/WS_2 moiré superlattices, Nature (London) **579**, 359 (2020).
[40] Z. Zhang, Y. Wang, K. Watanabe, T. Taniguchi, K. Ueno, E. Tutuc, and B. J. LeRoy, Flat bands in twisted bilayer transition metal dichalcogenides, Nat. Phys. **16**, 1093 (2020).
[41] L. Wang, E.-M. Shih, A. Ghiotto, L. Xian, D. A. Rhodes, C. Tan, M. Claassen, D. M. Kennes, Y. Bai, B. Kim,

K. Watanabe, T. Taniguchi, X. Zhu, J. Hone, A. Rubio, A. N. Pasupathy, and C. R. Dean, Correlated electronic phases in twisted bilayer transition metal dichalcogenides, Nat. Mater. **19**, 861 (2020).

[42] A. Ghiotto, E.-M. Shih, G. S. S. G. Pereira, D. A. Rhodes, B. Kim, J. Zang, A. J. Millis, K. Watanabe, T. Taniguchi, J. C. Hone, L. Wang, C. R. Dean, and A. N. Pasupathy, Quantum criticality in twisted transition metal dichalcogenides, Nature (London) **597**, 345 (2021).

[43] Q. Tong, F. Liu, J. Xiao, and W. Yao, Skyrmions in the moiré of van der Waals 2D magnets, Nano Lett. **18**, 7194 (2018).

[44] K. Hejazi, Z.-X. Luo, and L. Balents, Noncollinear phases in moiré magnets, Proc. Natl. Acad. Sci. U.S.A. **117**, 10721 (2020).

[45] O. Can, T. Tummuru, R. P. Day, I. Elfimov, A. Damascelli, and M. Franz, High-temperature topological superconductivity in twisted double-layer copper oxides, Nat. Phys. **17**, 519 (2021).

[46] Y. Zhu, M. Liao, Q. Zhang, H.-Y. Xie, F. Meng, Y. Liu, Z. Bai, S. Ji, J. Zhang, K. Jiang, R. Zhong, J. Schneeloch, G. Gu, L. Gu, X. Ma, D. Zhang, and Q.-K. Xue, Presence of *s*-wave pairing in Josephson junctions made of twisted ultrathin $Bi_2Sr_2CaCu_2O_{8+x}$ flakes, Phys. Rev. X **11**, 031011 (2021).

[47] P. A. Volkov, J. H. Wilson, K. P. Lucht, and J. H. Pixley, Magic angles and correlations in twisted nodal superconductors, Phys. Rev. B **107**, 174506 (2023).

[48] P. A. Volkov, J. H. Wilson, K. P. Lucht, and J. H. Pixley, Current- and field-induced topology in twisted nodal superconductors, Phys. Rev. Lett. **130**, 186001 (2023).

[49] S. Y. F. Zhao, X. Cui, P. A. Volkov, H. Yoo, S. Lee, J. A. Gardener, A. J. Akey, R. Engelke, Y. Ronen, R. Zhong, G. Gu, S. Plugge, T. Tummuru, M. Kim, M. Franz, J. H. Pixley, N. Poccia, and P. Kim, Time-reversal symmetry breaking superconductivity between twisted cuprate superconductors, Science **382**, 1422 (2023).

[50] A. González-Tudela and J. I. Cirac, Cold atoms in twisted-bilayer optical potentials, Phys. Rev. A **100**, 053604 (2019).

[51] Y. Fu, E. J. König, J. H. Wilson, Y.-Z. Chou, and J. H. Pixley, Magic-angle semimetals, npj Quantum Mater. **5**, 71 (2020).

[52] X.-W. Luo and C. Zhang, Spin-twisted optical lattices: Tunable flat bands and Larkin-Ovchinnikov superfluids, Phys. Rev. Lett. **126**, 103201 (2021).

[53] Z. Meng, L. Wang, W. Han, F. Liu, K. Wen, C. Gao, P. Wang, C. Chin, and J. Zhang, Atomic Bose–Einstein condensate in twisted-bilayer optical lattices, Nature (London) **615**, 231 (2023).

[54] P. O. Sukhachov, F. von Oppen, and L. I. Glazman, Tunneling spectra of impurity states in unconventional superconductors, Phys. Rev. B **108**, 024505 (2023).

[55] P. Haase, S. Fuchs, T. Pruschke, H. Ochoa, and F. Guinea, Magnetic moments and Kondo effect near vacancies and resonant scatterers in graphene, Phys. Rev. B **83**, 241408 (R) (2011).

[56] J. J. Palacios and F. Ynduráin, Critical analysis of vacancy-induced magnetism in monolayer and bilayer graphene, Phys. Rev. B **85**, 245443 (2012).

[57] B. R. K. Nanda, M. Sherafati, Z. S. Popović, and S. Satpathy, Electronic structure of the substitutional vacancy in graphene: Density-functional and Green's function studies, New J. Phys. **14**, 083004 (2012).

[58] J. Mao, Y. Jiang, D. Moldovan, G. Li, K. Watanabe, T. Taniguchi, M. R. Masir, F. M. Peeters, and E. Y. Andrei, Realization of a tunable artificial atom at a supercritically charged vacancy in graphene, Nat. Phys. **12**, 545 (2016).

[59] Y. Jiang, P.-W. Lo, D. May, G. Li, G.-Y. Guo, F. B. Anders, T. Taniguchi, K. Watanabe, J. Mao, and E. Y. Andrei, Inducing Kondo screening of vacancy magnetic moments in graphene with gating and local curvature, Nat. Commun. **9**, 2349 (2018).

[60] D. May, P.-W. Lo, K. Deltenre, A. Henke, J. Mao, Y. Jiang, G. Li, E. Y. Andrei, G.-Y. Guo, and F. B. Anders, Modeling of the gate-controlled Kondo effect at carbon point defects in graphene, Phys. Rev. B **97**, 155419 (2018).

[61] D. Withoff and E. Fradkin, Phase transitions in gapless Fermi systems with magnetic impurities, Phys. Rev. Lett. **64**, 1835 (1990).

[62] R. Bulla, T. Pruschke, and A. C. Hewson, Anderson impurity in pseudo-gap Fermi systems, J. Phys. Condens. Matter **9**, 10463 (1997).

[63] C. Gonzalez-Buxton and K. Ingersent, Renormalization-group study of Anderson and Kondo impurities in gapless Fermi systems, Phys. Rev. B **57**, 14254 (1998).

[64] K. Ingersent and Q. Si, Critical local-moment fluctuations, anomalous exponents, and ω/t scaling in the Kondo problem with a pseudogap, Phys. Rev. Lett. **89**, 076403 (2002).

[65] L. Fritz and M. Vojta, Phase transitions in the pseudogap Anderson and Kondo models: Critical dimensions, renormalization group, and local-moment criticality, Phys. Rev. B **70**, 214427 (2004).

[66] M. Vojta and L. Fritz, Upper critical dimension in a quantum impurity model: Critical theory of the asymmetric pseudogap Kondo problem, Phys. Rev. B **70**, 094502 (2004).

[67] L. Fritz, S. Florens, and M. Vojta, Universal crossovers and critical dynamics of quantum phase transitions: A renormalization group study of the pseudogap Kondo problem, Phys. Rev. B **74**, 144410 (2006).

[68] M. T. Glossop, S. Kirchner, J. H. Pixley, and Q. Si, Critical Kondo destruction in a pseudogap Anderson model: Scaling and relaxational dynamics, Phys. Rev. Lett. **107**, 076404 (2011).

[69] J. H. Pixley, S. Kirchner, K. Ingersent, and Q. Si, Quantum criticality in the pseudogap Bose-Fermi Anderson and Kondo models: Interplay between fermion- and boson-induced Kondo destruction, Phys. Rev. B **88**, 245111 (2013).

[70] L. Fritz and M. Vojta, The physics of Kondo impurities in graphene, Rep. Prog. Phys. **76**, 032501 (2013).

[71] J. H. Pixley, T. Chowdhury, M. T. Miecnikowski, J. Stephens, C. Wagner, and K. Ingersent, Entanglement entropy near Kondo-destruction quantum critical points, Phys. Rev. B **91**, 245122 (2015).

[72] C. Wagner, T. Chowdhury, J. H. Pixley, and K. Ingersent, Long-range entanglement near a Kondo-destruction quantum critical point, Phys. Rev. Lett. **121**, 147602 (2018).

[73] A. Cai, J. H. Pixley, K. Ingersent, and Q. Si, Critical local moment fluctuations and enhanced pairing correlations in a cluster Anderson model, Phys. Rev. B **101**, 014452 (2020).

[74] J.-H. Chen, L. Li, W. G. Cullen, E. D. Williams, and M. S. Fuhrer, Tunable Kondo effect in graphene with defects, Nat. Phys. **7**, 535 (2011).

[75] T. O. Wehling, A. M. Black-Schaffer, and A. V. Balatsky, Dirac materials, Adv. Phys. **63**, 1 (2014).

[76] A. S. Shankar, D. O. Oriekhov, A. K. Mitchell, and L. Fritz, Kondo effect in twisted bilayer graphene, Phys. Rev. B **107**, 245102 (2023).

[77] F. Dietrich, U. J. Guevara, A. Tiutiunnyk, D. Laroze, and E. Cisternas, Vacancies and Stone–Wales defects in twisted bilayer graphene—A comparative theoretical study, FlatChem **41**, 100541 (2023).

[78] S. Wang, A. Robertson, and J. H. Warner, Atomic structure of defects and dopants in 2D layered transition metal dichalcogenides, Chem. Soc. Rev. **47**, 6764 (2018).

[79] H. Guo, X. Zhang, and G. Lu, Moiré excitons in defective van der Waals heterostructures, Proc. Natl. Acad. Sci. U.S.A. **118**, e2105468118 (2021).

[80] S. H. Pan, E. W. Hudson, K. M. Lang, H. Eisaki, S. Uchida, and J. C. Davis, Imaging the effects of individual zinc impurity atoms on superconductivity in $Bi_2Sr_2CaCu_2O_{8+\delta}$, Nature (London) **403**, 746 (2000).

[81] H. Alloul, J. Bobroff, M. Gabay, and P. J. Hirschfeld, Defects in correlated metals and superconductors, Rev. Mod. Phys. **81**, 45 (2009).

[82] A. Weiße, G. Wellein, A. Alvermann, and H. Fehske, The kernel polynomial method, Rev. Mod. Phys. **78**, 275 (2006).

[83] R. Bulla, T. A. Costi, and T. Pruschke, Numerical renormalization group method for quantum impurity systems, Rev. Mod. Phys. **80**, 395 (2008).

[84] A.-K. Wu, D. Bauernfeind, X. Cao, S. Gopalakrishnan, K. Ingersent, and J. H. Pixley, Aubry-André Anderson model: Magnetic impurities coupled to a fractal spectrum, Phys. Rev. B **106**, 165123 (2022).

[85] R. Bistritzer and A. H. MacDonald, Moiré bands in twisted double-layer graphene, Proc. Natl. Acad. Sci. U.S.A. **108**, 12233 (2011).

[86] S. Pathak, T. Rakib, R. Hou, A. Nevidomskyy, E. Ertekin, H. T. Johnson, and L. K. Wagner, Accurate tight-binding model for twisted bilayer graphene describes topological flat bands without geometric relaxation, Phys. Rev. B **105**, 115141 (2022).

[87] See Supplemental Material at http://link.aps.org/supplemental/10.1103/PhysRevLett.133.126503, which includes Refs. [88–109], for additional information about the details of atomic-scale simulations, construction of the impurity model, discussions about emergent multifractality, and further details of numerical renormalization group calculations.

[88] G. Kresse and J. Hafner, *Ab initio* molecular dynamics for liquid metals, Phys. Rev. B **47**, 558 (1993).

[89] G. Kresse and J. Furthmüller, Efficiency of ab-initio total energy calculations for metals and semiconductors using a plane-wave basis set, Comput. Mater. Sci. **6**, 15 (1996).

[90] G. Kresse and J. Furthüller, Efficient iterative schemes for *ab initio* total-energy calculations using a plane-wave basis set, Phys. Rev. B **54**, 11169 (1996).

[91] J. P. Perdew, K. Burke, and M. Ernzerhof, Generalized gradient approximation made simple, Phys. Rev. Lett. **77**, 3865 (1996).

[92] P. A. Thrower and R. M. Mayer, Point defects and self-diffusion in graphite, Phys. Status Solidi (a) **47**, 11 (1978).

[93] M. Leccese and R. Martinazzo, Anomalous delocalization of resonant states in graphene & the vacancy magnetic moment, Electronic structure and magnetism of inorganic compounds **5**, 024010 (2023).

[94] V. G. Miranda, L. G. G. V. Dias Da Silva, and C. H. Lewenkopf, Coulomb charging energy of vacancy-induced states in graphene, Phys. Rev. B **94**, 075114 (2016).

[95] M. Schüler, M. Rösner, T. O. Wehling, A. I. Lichtenstein, and M. I. Katsnelson, Optimal Hubbard models for materials with nonlocal Coulomb interactions: Graphene, silicene, and benzene, Phys. Rev. Lett. **111**, 036601 (2013).

[96] H. J. Changlani, H. Zheng, and L. K. Wagner, Density-matrix based determination of low-energy model Hamiltonians from *ab initio* wavefunctions, J. Chem. Phys. **143**, 102814 (2015).

[97] N. Marzari and D. Vanderbilt, Maximally localized generalized Wannier functions for composite energy bands, Phys. Rev. B **56**, 12847 (1997).

[98] A. A. Mostofi, J. R. Yates, Y.-S. Lee, I. Souza, D. Vanderbilt, and N. Marzari, wannier90: A tool for obtaining maximally-localised Wannier functions, Comput. Phys. Commun. **178**, 685 (2008).

[99] A. A. Mostofi, J. R. Yates, G. Pizzi, Y.-S. Lee, I. Souza, D. Vanderbilt, and N. Marzari, An updated version of wannier90: A tool for obtaining maximally-localised Wannier functions, Comput. Phys. Commun. **185**, 2309 (2014).

[100] G. Pizzi *et al.*, Wannier90 as a community code: New features and applications, J. Phys. Condens. Matter **32**, 165902 (2020).

[101] V. Dobrosavljević, T. R. Kirkpatrick, and B. G. Kotliar, Kondo effect in disordered systems, Phys. Rev. Lett. **69**, 1113 (1992).

[102] E. Miranda, V. Dobrosavljević, and G. Kotliar, Kondo disorder: A possible route towards non-Fermi-liquid behaviour, J. Phys. Condens. Matter **8**, 9871 (1996).

[103] P. S. Cornaglia, D. R. Grempel, and C. A. Balseiro, Universal distribution of Kondo temperatures in dirty metals, Phys. Rev. Lett. **96**, 117209 (2006).

[104] S. Kettemann, E. R. Mucciolo, and I. Varga, Critical metal phase at the Anderson metal-insulator transition with Kondo impurities, Phys. Rev. Lett. **103**, 126401 (2009).

[105] V. G. Miranda, L. G. G. V. Dias da Silva, and C. H. Lewenkopf, Disorder-mediated Kondo effect in graphene, Phys. Rev. B **90**, 201101 (2014).

[106] E. C. Andrade, A. Jagannathan, E. Miranda, M. Vojta, and V. Dobrosavljević, Non-Fermi-liquid behavior in metallic quasicrystals with local magnetic moments, Phys. Rev. Lett. **115**, 036403 (2015).

[107] A. M. Coe, G. Li, and E. Y. Andrei, Cryogen-free modular scanning tunneling microscope operating at 4-K in high magnetic field on a compact ultra-high vacuum platform, arXiv:2404.05002.

[108] R. Peters, T. Pruschke, and F. B. Anders, Numerical renormalization group approach to Green's functions for

quantum impurity models, Phys. Rev. B **74**, 245114 (2006).
[109] A. Weichselbaum and J. von Delft, Sum-rule conserving spectral functions from the numerical renormalization group, Phys. Rev. Lett. **99**, 076402 (2007).
[110] D. W. Brenner, O. A. Shenderova, J. A. Harrison, S. J. Stuart, B. Ni, and S. B. Sinnott, A second-generation reactive empirical bond order (REBO) potential energy expression for hydrocarbons, J. Phys. Condens. Matter **14**, 783 (2002).
[111] A. N. Kolmogorov and V. H. Crespi, Registry-dependent interlayer potential for graphitic systems, Phys. Rev. B **71**, 235415 (2005).
[112] W. Ouyang, D. Mandelli, M. Urbakh, and O. Hod, Nanoserpents: Graphene nanoribbon motion on two-dimensional hexagonal materials, Nano Lett. **18**, 6009 (2018).
[113] T. Rakib, P. Pochet, E. Ertekin, and H. T. Johnson, Corrugation-driven symmetry breaking in magic-angle twisted bilayer graphene, Commun. Phys. **5**, 242 (2022).
[114] K. Krongchon, T. Rakib, S. Pathak, E. Ertekin, H. T. Johnson, and L. K. Wagner, Registry-dependent potential energy and lattice corrugation of twisted bilayer graphene from quantum Monte Carlo, Phys. Rev. B **108**, 235403 (2023).
[115] A. P. Thompson, H. M. Aktulga, R. Berger, D. S. Bolintineanu, W. M. Brown, P. S. Crozier, P. J. in 't Veld, A. Kohlmeyer, S. G. Moore, T. D. Nguyen, R. Shan, M. J. Stevens, J. Tranchida, C. Trott, and S. J. Plimpton, LAMMPS—a flexible simulation tool for particle-based materials modeling at the atomic, meso, and continuum scales, Comput. Phys. Commun. **271**, 108171 (2022).
[116] S. Dai, Y. Xiang, and D. J. Srolovitz, Twisted bilayer graphene: Moiré with a twist, Nano Lett. **16**, 5923 (2016).
[117] K. Zhang and E. B. Tadmor, Structural and electron diffraction scaling of twisted graphene bilayers, J. Mech. Phys. Solids **112**, 225 (2018).
[118] P. Lucignano, D. Alfè, V. Cataudella, D. Ninno, and G. Cantele, Crucial role of atomic corrugation on the flat bands and energy gaps of twisted bilayer graphene at the magic angle $\theta \sim 1.08°$, Phys. Rev. B **99**, 195419 (2019).
[119] H. Yoo, R. Engelke, S. Carr, S. Fang, K. Zhang, P. Cazeaux, S. H. Sung, R. Hovden, A. W. Tsen, T. Taniguchi, K. Watanabe, G.-C. Yi, M. Kim, M. Luskin, E. B. Tadmor, E. Kaxiras, and P. Kim, Atomic and electronic reconstruction at the van der Waals interface in twisted bilayer graphene, Nat. Mater. **18**, 448 (2019).
[120] The spin ↑ or ↓, given by a spin-polarized calculation, does not correspond to any real-space direction.
[121] Here, k labels the eigenstate, but does not represent the momentum. The lattice model is defined on an incommensurate lattice. Therefore, momentum is not a well-defined quantum number.
[122] J. H. Wilson, Y. Fu, S. Das Sarma, and J. H. Pixley, Disorder in twisted bilayer graphene, Phys. Rev. Res. **2**, 023325 (2020).
[123] S. Carr, S. Fang, Z. Zhu, and E. Kaxiras, Exact continuum model for low-energy electronic states of twisted bilayer graphene, Phys. Rev. Res. **1**, 013001 (2019).
[124] H. C. Po, L. Zou, T. Senthil, and A. Vishwanath, Faithful tight-binding models and fragile topology of magic-angle bilayer graphene, Phys. Rev. B **99**, 195455 (2019).
[125] S. Carr, S. Fang, H. C. Po, A. Vishwanath, and E. Kaxiras, Derivation of Wannier orbitals and minimal-basis tight-binding Hamiltonians for twisted bilayer graphene: First-principles approach, Phys. Rev. Res. **1**, 033072 (2019).
[126] S. Carr, S. Fang, and E. Kaxiras, Electronic-structure methods for twisted moiré layers, Nat. Rev. Mater. **5**, 748 (2020).
[127] K. Chen and C. Jayaprakash, The Kondo effect in pseudo-gap Fermi systems: A renormalization group study, J. Phys. Condens. Matter **7**, L491 (1995).
[128] M. Filippone, C. P. Moca, A. Weichselbaum, J. von Delft, and C. Mora, At which magnetic field, exactly, does the Kondo resonance begin to split? A Fermi liquid description of the low-energy properties of the Anderson model, Phys. Rev. B **98**, 075404 (2018).
[129] S. Kettemann, E. R. Mucciolo, I. Varga, and K. Slevin, Kondo-Anderson transitions, Phys. Rev. B **85**, 115112 (2012).
[130] R. Gammag and K.-S. Kim, Distribution of critical temperature at Anderson localization, Phys. Rev. B **93**, 205128 (2016).
[131] K. Slevin, S. Kettemann, and T. Ohtsuki, Multifractality and the distribution of the Kondo temperature at the Anderson transition, Eur. Phys. J. B **92**, 281 (2019).
[132] M. Gonçalves, H. Z. Olyaei, B. Amorim, R. Mondaini, P. Ribeiro, and E. V. Castro, Incommensurability-induced sub-ballistic narrow-band-states in twisted bilayer graphene, 2D Mater. **9**, 011001 (2021).
[133] X. Lu, P. Stepanov, W. Yang, M. Xie, M. A. Aamir, I. Das, C. Urgell, K. Watanabe, T. Taniguchi, G. Zhang, A. Bachtold, A. H. MacDonald, and D. K. Efetov, Superconductors, orbital magnets and correlated states in magic-angle bilayer graphene, Nature (London) **574**, 653 (2019).
[134] Http://oarc.rutgers.edu.
[135] A. Weichselbaum, Non-Abelian symmetries in tensor networks: A quantum symmetry space approach, Ann. Phys. (Amsterdam) **327**, 2972 (2012); Tensor networks and the numerical renormalization group, Phys. Rev. B **86**, 245124 (2012); X-symbols for non-Abelian symmetries in tensor networks, Phys. Rev. Res. **2**, 023385 (2020).
[136] S.-S. B. Lee and A. Weichselbaum, Adaptive broadening to improve spectral resolution in the numerical renormalization group, Phys. Rev. B **94**, 235127 (2016).
[137] S.-S. B. Lee, J. von Delft, and A. Weichselbaum, Doublon-Holon origin of the subpeaks at the Hubbard band edges, Phys. Rev. Lett. **119**, 236402 (2017).
[138] S.-S. B. Lee, F. B. Kugler, and J. von Delft, Computing local multipoint correlators using the numerical renormalization group, Phys. Rev. X **11**, 041007 (2021).